Goethals, M. M., Hetzel, R., Niedermann, S., Wittmann, H., Fenton, C. R., Kubik, P. W., Christl, M., von Blanckenburg, F. (2009): An improved experimental determination of cosmogenic 10Be/21Ne and 26Al/21Ne production ratios in quartz. - Earth and Planetary Science Letters, 284, 1-2, 187-198

DOI: 10.1016/j.epsl.2009.04.027

An improved experimental determination of cosmogenic $^{10}Be/^{21}Ne$ and $^{26}Al/^{21}Ne$ production ratios in quartz

M.M. Goethals [a,b], R. Hetzel [a,*], S. Niedermann [b], H. Wittmann [b,c], C.R. Fenton [b,d], P.W. Kubik [e], M. Christl [e], F. von Blanckenburg [b,c]

[a] Geologisch-Paläontologisches Institut, Westfälische Wilhelms-Universität Münster, Corrensstr. 24, D-48149 Münster, Germany
[b] Helmholtz-Zentrum Potsdam – Deutsches GeoForschungsZentrum, Telegrafenberg, D-14473Potsdam, Germany (present address of F. von Blanckenburg and H. Wittmann)
[c] Institut für Mineralogie, Universität Hannover, Callinstrasse 3, D-30167 Hannover, Germany
[d] Scottish Universities Environmental Research Centre (SUERC), Scottish Enterprise Technology Park, Rankine Avenue, East Kilbride G75 0QF, United Kingdom (present address of C.R. Fenton)
[e] Laboratory of Ion Beam Physics ETH Zurich, CH-8093 Zurich, Switzerland

* Corresponding author: Ralf Hetzel, Geologisch-Paläontologisches Institut, WestfälischeWilhelms-Universität Münster, Corrensstr. 24, D-48149 Münster, Germany
Phone: +49 251 8333908; Fax: +49 251 8333968

E-mail addresses: mirjamgoethals@yahoo.com (M.M. Goethals), rahetzel@uni-muenster.de (R. Hetzel), nied@gfz-potsdam.de (S. Niedermann), wittmann@gfz-potsdam.de (H. Wittmann), c.fenton@suerc.gla.ac.uk (C.R. Fenton), kubik@phys.ethz.ch (P.W. Kubik), christl@phys.ethz.ch (M. Christl), fvb@gfz-potsdam.de (F. von Blanckenburg).

Abstract
The confidence in surface exposure dating and related research, such as erosion rate studies or burial dating, strongly depends on the accuracy and precision of the currently used production rates of in situ-produced cosmogenic nuclides. Reducing the uncertainties of nuclide production rates by more accurate calibrations with independently dated natural rock surfaces is crucial for further improving the quantification of earth surface processes. Here we use surface samples from the 760±2 ka old Bishop Tuff in eastern California to quantify the $^{10}Be/^{21}Ne$ and $^{26}Al/^{21}Ne$ production rate ratios in quartz. Our determination is based on (1) measured nuclide concentrations of cosmogenic ^{10}Be, ^{21}Ne, and ^{26}Al, (2) a conservative estimate for the erosion of the tuff in the Volcanic Tableland area, which we base on our previously published ^{21}Ne concentrations (Goethals et al., 2009) and a conservative estimate for the uncertainty of the ^{21}Ne production rate, and (3) the assumption of steady-state erosion. Other assumptions, such as the applied scaling procedure, the muon contribution to nuclide production, or the attenuation lengths of neutrons and muons in rock, do not substantially affect the results. Based on 13 samples, the following average production rate ratios and conservative uncertainty estimates are obtained for sea level, high latitude, open sky, and rock surface: 0.249±0.009 or 0.232±0.009 for $^{10}Be/^{21}Ne$ using ^{10}Be half-lives of 1.51 and 1.39 Ma, respectively, and 1.80±0.09 for $^{26}Al/^{21}Ne$ (for an ^{26}Al half-life of 0.72 Ma). The $^{10}Be/^{21}Ne$ and the $^{26}Al/^{21}Ne$ production ratios are consistent with currently used production rates but the ratios are much more precise than previous determinations. The resulting $^{26}Al/^{10}Be$ production ratio of 7.23±0.45 (for a ^{10}Be half-life of 1.51 Ma) or 7.76±0.49 (for a ^{10}Be half-life of 1.39 Ma) is high when compared to previously published values. We discuss reasons for this difference, amongst them the possibility that ^{26}Al analyses in general might be compromised by artefacts affecting the stable Al concentration measurements. When combined with a ^{10}Be production rate of 5.01 at g^{-1} a^{-1} for the 1.51 Ma half-life (or 4.61 at g^{-1} a^{-1} for the 1.39 Ma half-life), our production ratios convert to ^{21}Ne and ^{26}Al production rates of 20.1 and 36.2 at g^{-1} a^{-1} (or 19.9 and 35.7 at g^{-1} a^{-1}), respectively.

Keywords: Cosmogenic nuclide (^{10}Be,^{21}Ne,^{26}Al), production rate, erosion island plot

1. Introduction

Exposure ages and erosion rates derived from cosmogenic nuclides are, in the best case, as accurate as the production rates they rely on. Although both experimental determinations and model calculations are available for the production rates of commonly used cosmogenic nuclides, their accuracy is limited by, e.g., the difficulty of obtaining suitable independently dated material, the intricacies involved in scaling from one location on the earth's surface to another one, or the limited knowledge on nuclear excitation functions for neutron-induced spallation reactions, and is usually estimated at ~10-20%. While the number of different experimental production rate determinations is rather large for ^{3}He in olivine and ^{10}Be in quartz (e.g. Gosse and Phillips, 2001; Licciardi et al., 2006; Balco et al., 2008), the database for ^{26}Al and ^{36}Cl is considerably smaller, and there has only been

one single value for ^{21}Ne in quartz until very recently (Niedermann et al., 1994; revised by Niedermann, 2000); an additional study reporting an independently determined ^{21}Ne production rate (Balco and Shuster, 2009) has just appeared. As the accuracy of a production rate is expected to increase with the number of independent determinations (under the assumption that deviations are mainly of statistical nature), it could be favourable to link poorly known production rates to those with better confidence, e.g. those of ^{21}Ne and ^{26}Al in quartz to that of ^{10}Be in the same mineral. In other words, instead of determining all production rates individually, it would suffice to know a single one of them absolutely, while only accurate production rate *ratios* would be needed for the other ones.

Indeed, production rate ratios have already been reported in the earliest studies dealing with production rate determinations in quartz: Nishiizumi et al. (1989) obtained a mean ^{26}Al/^{10}Be production ratio of 6.02±0.44 (1σ) from ten glacially polished granite surfaces sampled in the Sierra Nevada, California. Later Niedermann et al. (1994) measured ^{21}Ne in two of the same samples, yielding a ^{21}Ne/^{26}Al production ratio of 0.65±0.11. However, since these ratios were determined in rather young (~13 ka) samples, their precision is limited due to low cosmogenic nuclide concentrations, and the same holds for subsequent studies of this kind (e.g. Kubik et al., 1998). In principle, production rate ratios can be determined in any sample in which more than one cosmogenic nuclide is measured, provided that a single-stage exposure history with no erosion is ensured. Whenever erosion or any other change in exposure conditions is involved, the production ratio of two cosmogenic nuclides can no longer easily be calculated from their concentration ratio and their half-lives (unless both nuclides are stable). In practice, this has been a serious obstacle to accurate determinations of ^{10}Be-^{21}Ne-^{26}Al production ratios, because it is rarely possible to exclude changing irradiation conditions for old samples, whereas for younger samples the precision of nuclide concentration measurements is often not sufficient, especially for ^{21}Ne.

Here we show that erosion does not necessarily preclude a determination of the ^{10}Be-^{21}Ne-^{26}Al production ratios, provided that some constraint on the erosion rate is available. Our samples originate from the Volcanic Tableland in the southeastern part of the Bishop Tuff, an ignimbrite erupted from Long Valley Caldera (California) 760±2 ka ago as established by ^{40}Ar/^{39}Ar dating (van den Bogaard and Schirnick, 1995), where we carried out an erosion study based on cosmogenic ^{21}Ne in quartz (Goethals et al., 2009). The precise age of the tuff, which was confirmed by Sarna-Wojcicki et al. (2000), along with high cosmogenic nuclide concentrations in the quartz allow us to use the same samples to determine precise production ratios of ^{10}Be/^{21}Ne and ^{26}Al/^{21}Ne. To do so, we only need to make a conservative assumption for the absolute ^{21}Ne production rate in order to set limits on the erosion of the studied surfaces.

2. Geological, geomorphological and climatic setting of the Bishop Tuff area

The Bishop Tuff (Figure 1) is an ignimbrite that erupted during the formation of the Long Valley Caldera in eastern California (e.g. Wilson and Hildreth, 2003). The tuff lies in the rainshadow of the Sierra Nevada, the mountain range west of the tuff, and it is situated in the northern part of Owens Valley just north of the town of Bishop. In the east, the Bishop Tuff is bordered by the White Mountains, the easternmost range of the Basin and Range Province.

The Bishop Tuff area has a desert climate and a vegetation of scattered small bushes and scrubs. In the south-eastern part of the Bishop Tuff, known as the Volcanic Tableland, the uppermost part of the tuff consists of a 40 to 80-m-thick ignimbrite unit referred to as Ig2Eb by Wilson and Hildreth (1997). The rocks contain abundant pumice and rhyolite lithics with ortho- and clinopyroxene phenocrysts, sanidine, magnetite (Wilson and Hildreth, 1997), and quartz phenocrysts up to 3 mm in size, with a mean diameter of 1-2 mm. The ignimbrite unit is increasingly welded towards the top and has a remarkably flat, low relief surface at around 1400 m elevation. Erosion of the Bishop Tuff surface in the sampled area of the Volcanic Tableland has been assessed based on ^{21}Ne concentrations in quartz samples, showing that (under the assumption of steady state erosion) 85-320 cm of the surface have been removed from the sample sites since the eruption 760 ka ago (Goethals et al., 2009).

3. Experimental procedures

3.1 Sampling and quartz separation

Ignimbrite samples were taken from both bedrock and desert pavement on the erosion-resistant surface of the Ig2Eb unit of the Volcanic Tableland (Goethals et al., 2009). For this study, only a subset of the bedrock samples was used (Table 1); desert pavement samples were discarded because they represent mixtures of clasts, each of which may have experienced a different irradiation history. Images of the sample sites are shown in Fig. S1 in the electronic supplement and in Goethals et al. (2009). Most of the investigated samples were taken from the subhorizontal part of the footwalls of normal faults, several metres away from the steep fault scarps, or in areas not affected by faulting. The relatively high sampling sites in the uplifted footwall blocks were least likely covered by local alluvium, and were presumably blown free of snow first in colder periods. Two samples (05BT16 and –17) were taken from bedrock exposures in ephemeral streams to assess the maximum amount of erosion in this part of the Volcanic Tableland. The maximum sample thickness was 4 cm. At all sampled sites

the production of cosmogenic nuclides was only negligibly reduced by the surrounding mountains (at most 0.04%), hence no correction for horizon shielding was applied. We also did not apply a correction for snow cover. Even though it is difficult to achieve a realistic estimate of the snow cover in the Volcanic Tableland over the last 760 ka, its influence on the cosmogenic nuclide concentrations is probably limited to <3%. For example, assuming that during half of the lifetime of the Bishop Tuff there may have been 0.5 m of snow (density 0.3 g cm^{-3}) for 6 months in a year, the ^{21}Ne concentration would be reduced by just 2.2%; ratios of two cosmogenic nuclides would be even less influenced. During the late Wisconsin glacial stage (~20 ka ago), low elevation areas west of the White Mountains down to the elevation of the Bishop Tuff were dominated by juniper woodlands associated with a xeric assemblage of understory shrubs (Jennings and Elliott-Fisk, 1993). Therefore, a cover by ice during glacial stages is unlikely in the Volcanic Tableland. We also did not apply a shielding correction for vegetation, because the biomass stored in juniper woodlands is considerably smaller than that of an acadian/boreal forest, for which a long-term shielding of ~2.3% has been estimated (Plug et al., 2007).
All rock samples were crushed, washed and sieved. The 315-710 µm and 710-1000 µm grain size fractions were split into magnetic and non-magnetic fractions using a Frantz magnetic separator. The non-magnetic fraction (sanidine, quartz) was treated and purified according to procedures introduced by Kohl and Nishiizumi (1992). This treatment involved a first leach in 6M HCl at a temperature of ~80°C, followed by several leaching steps in dilute HF/HNO_3 in a hot ultrasonic bath (80°C) (see Hetzel et al., 2002 for details) during which sanidine is dissolved and meteoric ^{10}Be is removed from quartz surfaces. The remaining quartz was used for all Ne analyses. For the Al and Be analyses, samples were further purified in aqua regia and HF (~10%) solutions at approximately 100°C, until the Al concentration was <300 ppm. On average the samples had three aqua regia and three HF treatments, alternated, with a final average Al concentration in quartz of about 130 ppm.

3.2 Neon analysis
Noble gases were analysed at Deutsches GeoForschungsZentrum (GFZ) in Potsdam using a VG5400 noble gas mass spectrometer. About 0.5-0.7 g of purified quartz were wrapped in Al-foil and heated to extract the noble gases in three or four different temperature steps of 400, (600), 800 and 1200°C. Further details about the analytical procedures and data reduction methods can be found in Niedermann et al. (1997) and Goethals et al. (2009). To relate our ^{21}Ne data to those obtained in other labs, we have measured six aliquots of the quartz standard CREU-1 that was distributed within the CRONUS-EU project. We obtain a mean ^{21}Ne excess of $(328\pm8) \times 10^6$ at g^{-1} by stepwise heating up to 1200°C.

3.3 Be and Al separation and AMS analysis
Beryllium and aluminium have been extracted from quartz using the method described by Stone (http://depts.washington.edu/cosmolab/chem.html). About 10 g of quartz were weighed and 0.3 to 0.4 mg Be was added from ^{9}Be carrier solutions. In the course of this study two ^{9}Be carrier solutions were used; both were prepared by one of the authors (FvB) from a phenakite crystal obtained from a deep mine in the Urals, Russia. Both carrier solutions were calibrated independently from each other and the results do not depend on the used carrier (see section 5.2). After complete dissolution of the quartz in HF (40%), a mixture of ~50 ml HF and concentrated HCl was added in a ratio of 4:1, and two to four aliquots (2 ml each) were used to determine the natural aluminium contents with ICP-OES (section 3.5). The remaining HF/HCl sample solution was evaporated before the sample was re-dissolved and run through successive anion and cation exchange columns. Be and Al in the eluates were precipitated as hydroxides at a pH of 8-9 and 7-8, respectively (Ochs and Ivy-Ochs, 1997), rinsed, dried, and finally transformed to BeO and Al_2O_3 at ~1000°C. Subsequently, the Be and Al oxides were mixed with copper powder and packed into AMS-cathodes in Münster, and were analysed at the AMS facility at ETH Zurich. The ETH ^{10}Be AMS standard S555 is a secondary standard calibrated to the ETH standard material BEST433, which was described in the publication reporting the determination of a ^{10}Be half-life of 1.51 Ma (Hofmann et al., 1987). The ETH ^{26}Al AMS standard ZAL94 is calibrated against the ^{26}Al AMS standard AL09 of the University of Cologne (Sarafin, 1985), whose ^{26}Al/Al ratio was calculated using a half-life of 0.72 Ma.

3.4 ^{10}Be half-life
While absolute radionuclide production ratios do not depend on assumptions on the nuclides' half-life, the AMS measurements do, given that they rely on an activity measurement made to determine the number of ^{10}Be atoms in the ^{10}Be/^{9}Be calibration standard or the number of ^{26}Al atoms in the ^{26}Al/^{27}Al standard, respectively. The commonly used 1.51 Ma half-life of ^{10}Be is currently under debate (e.g. Granger, 2006). Several new half-life determinations have suggested lower values around 1.36-1.41 Ma (Fink and Smith, 2007; Nishiizumi et al., 2007), and two recent studies have reached agreement, using different methods, at a half life of 1.39 Ma with an uncertainty of only ~1% (Chmeleff et al., 2009; Korschinek et al., 2009). Because in the past, most ^{10}Be AMS measurements have been based on AMS standards associated with a ^{10}Be half-life of 1.51 Ma, we shall present the ^{10}Be data in this paper for half-lives of both 1.51 Ma (Hofmann et al., 1987), to enable easy comparability with earlier work, and 1.39 Ma (Chmeleff et al., 2009; Korschinek et al., 2009), to comply with the most recent

state of the art. To convert measured ^{10}Be concentrations from the 1.51 Ma to the 1.39 Ma half-life, they must be multiplied by the ratio of the two half-lives (1.39/1.51), which reduces them by ~8%. Likewise, ^{10}Be production rate values which have been determined with young calibration samples (i.e., for which ^{10}Be decay is insignificant; e.g. Nishiizumi et al., 1989; Kubik et al., 1998) assuming a 1.51 Ma half-life will be reduced by 8%.

3.5 Stable aluminium analysis

The concentration of stable ^{27}Al in the quartz samples must be known to calculate the ^{26}Al concentration from the ^{26}Al/^{27}Al ratio measured by AMS. The Al concentrations of all samples have been determined by ICP-OES at the University of Hannover, applying the standard addition method to minimize matrix effects. The 2 ml aliquots taken after complete dissolution of the quartz samples were evaporated at 100°C, and were then stored in 6M HCl. Shortly before the ICP-OES analysis, the HCl solution was evaporated and the samples were re-dissolved in 4M HNO_3. Each aliquot was subsequently diluted and split into 5 or 6 equal volumes, and increasing amounts of Al standard solution – prepared from a commercially available Merck® standard – were added gravimetrically. The initial Al concentration of the aliquot in the analyte solutions was about 0.4-0.7 ppm and the addition of the Al standard resulted in added concentrations of 0.1, 0.2, 0.3, 0.4, and 1.0 ppm Al in addition to the 'aliquot Al'. Finally, 0.3 M HNO_3 was added - taking dilution into account - to reach the analyte volume of ~5 ml required for ICP-OES analysis. We assumed an error of 1% on the Al concentration of each added standard solution to account for uncertainties from weighing, evaporation, and the Al concentration of the commercial standard. For the Al analysis the 167.019 nm wavelength was used, which is particularly sensitive at low Al concentrations due to its high signal to background ratio and good ionization qualities (Schulz and Heitland, 2001). After the ICP-OES analysis, the average signal (counts s^{-1}) of 4 or 5 replicate measurements was corrected for background, and the corresponding standard deviation for the replicate intensities was calculated. The ICP-OES results were evaluated using Isoplot3 software (Ludwig, 2003; Figure 2). At least three of the standard additions were used for regression analysis; additions that significantly deviated from the regression line – resulting in a 'probability of fit' of 0 – were not considered in the calculation (Table 2). Procedural blanks (n = 4) – including Be-carrier and acid additions – were always below 1% of the sample Al concentrations, hence no further blank corrections were applied.

Owing to the difficulty of accurately measuring Al concentrations (e.g. Gosse and Phillips, 2001; Bierman and Caffee, 2002; Bennett et al., 2005), we analysed a duplicate set of five aliquots at GFZ Potsdam. These aliquots were taken from the same dissolved quartz solutions as the aliquots analysed in Hannover. In Potsdam, the Al analyses were also carried out with the standard addition procedure, but on less diluted sample solutions (ICP-analyte concentration ~3-9 ppm) and using the 396.152 nm wavelength. The standard addition results obtained in Potsdam are in excellent agreement with the Hannover results (Table 2). Additionally, we tested the standard addition method by applying it to standard reference material. Three splits of the powder reference material (granite MA-N, GIT-IWT, SARM; Govindaraju, 1980; Govindaraju and Roelandts, 1993) with a concentration of 17.62±0.12 wt.% Al_2O_3 were dissolved and analysed with standard addition. The resulting concentrations of 17.54±0.55, 17.23±0.40 and 17.23±0.93 wt% Al_2O_3 are in very good agreement with the published value. Moreover, the five duplicate aliquots have also been analysed for Al by using an ordinary calibration curve. This approach yielded Al concentrations that are consistently lower, by 7 to 11%, than those obtained by standard addition. The reason for this discrepancy is most likely matrix effects, which are not accounted for by the ordinary calibration method.

To calculate the ^{26}Al concentrations in the Bishop Tuff quartz samples, we used the results of the ICP-OES analysis performed in Hannover on the 167.019 nm wavelength by the standard addition method, which is judged most accurate at the relevant concentration level (Schulz and Heitland, 2001). Nevertheless, the effect of a hypothetical lower Al concentration on the determined production rate ratios will be discussed in section 5.2.

4. Results

The concentrations of cosmogenic ^{21}Ne, ^{10}Be (for half-lives of 1.51 and 1.39 Ma, respectively) and ^{26}Al are presented in Table 3. All error limits correspond to the 95% confidence level. For ^{21}Ne, they include statistical uncertainties of the measurement, uncertainties of sensitivity and mass discrimination, and of blank and isobaric interference corrections. For ^{10}Be and ^{26}Al they include statistical errors and the uncertainties of the AMS standard values (5% for the Be standard S555 and 10% for the Al standard ZAL94 at the 2σ level) and for ^{10}Be also the uncertainty of the blank correction. The ^{26}Al concentrations also include the errors associated with the stable Al analysis. Due to the relatively high ^{10}Be concentrations in the samples, the blank correction (^{9}Be carrier) reduced them by only 0.17-0.70%. A blank (carrier) correction for ^{26}Al was not required, as the natural aluminium content of the quartz was used as an internal carrier and four blanks contained negligible amounts of Al.

4.1 Paired nuclide data

To assess a possible influence of erosion or temporary cover on our data we have, in a first step, plotted them in $^{21}Ne/^{10}Be$ versus ^{10}Be (Figure 3a) and $^{26}Al/^{10}Be$ versus ^{10}Be diagrams (Figure 3b), commonly referred to as "erosion island plots". These were constructed with CosmoCalc, version 1.4 (Vermeesch, 2007) using the parameters described hereafter. For the production rate of ^{10}Be (P_{10}) we used the "reference production rate for spallation" from Balco et al. (2008) for the Dunai (2000) scaling method, i.e. 4.90 at g^{-1} a^{-1} at sea level and high latitude, and added a contribution of 0.106 at g^{-1} a^{-1} (Heisinger et al., 2002a) by stopped muon interactions, i.e. a total P_{10} of 5.01 at g^{-1} a^{-1}. For the ^{21}Ne production rate (P_{21}), we used 19.0 at g^{-1} a^{-1} (Niedermann, 2000). The ^{26}Al production rate (P_{26}) data set in Balco et al. (2008) stems from only three sites within a small geographical extension. Therefore we prefer to combine the above P_{10} value with the experimental P_{26}/P_{10} ratio of 6.52 (Kubik et al., 1998), yielding P_{26} = 32.6 at g^{-1} a^{-1}. This method also avoids inconsistencies arising from different ^{26}Al standards used.

As the positions of the curves in the erosion island plots (Figure 3), which are scaled to sea level and high latitude, depend on the chosen values for production rates, half-lives, etc., they may vary within certain ranges according to the uncertainties of these parameters. Owing to the large data base (Balco et al., 2008), P_{10} is probably the best constrained among the production rates treated here. Therefore we illustrate the uncertainty in the position of the ^{21}Ne-^{10}Be steady state erosion island by considering the 2σ error limits of P_{21} of ±3.7 at g^{-1} a^{-1} (Niedermann, 2000), i.e. 22.7 and 15.3 at g^{-1} a^{-1}, but leaving P_{10} constant (Figure 3a). Likewise, for plotting the ^{26}Al-^{10}Be diagram (Figure 3b) we use the 2σ uncertainty range of the P_{26}/P_{10} ratio of ±0.86 (Kubik et al., 1998), yielding upper and lower P_{26} error limits of 36.9 and 28.3 at g^{-1} a^{-1}. The decay constants of ^{10}Be and ^{26}Al are 4.59×10^{-7} a^{-1} and 9.63×10^{-7} a^{-1}, respectively, corresponding to half-lives of 1.51 and 0.72 Ma. The method of Dunai (2000) was applied in scaling the nuclide concentrations to sea level and high latitude, and the algorithm of Granger and Smith (2000) was chosen from the CosmoCalc settings for the depth dependence of muon-induced production pathways. We used a rock density of 1.65 g cm^{-3} as determined experimentally for a Bishop Tuff sample (Goethals et al., 2009). Error bars for the samples in the erosion island plots are 2σ. For the ^{10}Be half-life of 1.39 Ma we do not show a separate erosion island plot, since both the data and the evolution lines would shift similarly in the region of interest.

In Figure 3a the scaled values of nearly all samples fall between the two pairs of lines that bound the steady state erosion field for P_{10} = 5.01 at g^{-1} a^{-1} and for P_{21} = 19.0 and 22.7 at g^{-1} a^{-1}, respectively. Although the majority of data tend to plot somewhat above the steady state erosion island corresponding to P_{21} = 19.0 at g^{-1} a^{-1}, this variation may be due to a somewhat higher P_{21} than proposed by Niedermann (2000) and is most likely not related to other factors such as burial. This inference is substantiated by geological evidence: A suggested intermittent cover could be a layer of ash and lapilli that covered the entire area after eruption of the Bishop Tuff. Such a cover should have a similar effect on samples that were taken from within 3 m of each other. Paired nuclide concentrations in such sample clusters (e.g. 05BT4, -6 or 05BT18, -19) do not reflect this, as data from the same cluster plot in considerably different positions relative to the steady state erosion field for P_{21} = 19.0 at g^{-1} a^{-1}. Consequently it is presumed that the samples did not experience a burial history that could have affected the cosmogenic nuclide production. In the $^{26}Al/^{10}Be$ versus ^{10}Be diagram (Figure 3b), most samples plot between the two pairs of lines that delimit the steady state erosion island for P_{10} = 5.01 at g^{-1} a^{-1} and P_{26} = 32.6 and 36.9 at g^{-1} a^{-1}. The fact that these data plot clearly away from the complex exposure history field is another argument against temporary burial.

4.2 The effect of erosion on nuclide ratios

While temporary burial is not an important issue for the Bishop Tuff samples, erosion certainly is (Goethals et al., 2009). For a surface with a given age and a simple exposure history, like the Bishop Tuff, the relation between the measured concentrations of two cosmogenic nuclides and their production rates depends only on the erosion rate. Erosion acts to remove part of the nuclides that were formed during surface exposure and thus changes the concentration ratio of two nuclides with different half-lives. The relation between P_j/P_{21} and C_j/C_{21} (where j = 10 for ^{10}Be or j = 26 for ^{26}Al and subscript 21 indicating ^{21}Ne) can be expressed by a factor f:

$$f = \frac{\left(P_j / P_{21}\right)}{\left(C_j / C_{21}\right)} \quad (1)$$

For the Bishop Tuff surface (eruption age 760 ka) and for fixed parameters of decay constants, neutron and muon production fractions and attenuation lengths, f depends only on erosion (see below and Figure 4). The erosion rate for each of the Bishop Tuff samples has been quantified based on ^{21}Ne concentrations in the quartz, assuming steady state erosion and using the ^{21}Ne sea level, high latitude production rate in quartz of 19.0 at g^{-1} a^{-1} (Niedermann, 2000) and a rock density of 1.65 g/cm^3 (Goethals et al., 2009). The resulting erosion rates for the samples used here range from ~140 to 420 cm Ma^{-1}, not including the uncertainty associated with the ^{21}Ne

production rate. As ignimbrites may have a varying density, e.g. depending on the welding degree that varies throughout the Bishop Tuff (Wilson and Hildreth, 2003), it is better to relate the factor f to the "mass removal rate" η (g cm^{-2} Ma^{-1}), i.e. the product of density ρ (g cm^{-3}) and erosion rate ε (cm Ma^{-1}). This way, our considerations will be completely independent of density variations.
Using the general solution of the differential equation describing the temporal evolution of a cosmogenic nuclide concentration in a steadily eroding rock (e.g., equation (27) in Niedermann, 2002) but neglecting production by cosmic ray muons in a first step, we obtain the following expression for factor f:

$$f = \frac{\left(\lambda_j \Lambda + \eta\right) \cdot \left(1 - e^{-\frac{\eta}{\Lambda} t}\right)}{\eta \left(1 - e^{-\left(\lambda_j + \frac{\eta}{\Lambda}\right) t}\right)} \quad (2)$$

where λ_j (j = 10 or 26) is the decay constant of ^{10}Be or ^{26}Al (Ma^{-1}), Λ is the effective cosmic ray spallation attenuation length in rock (g cm^{-2}), and t is the exposure time (0.76 Ma). The general equation which includes the production paths by negative muon capture and fast muon interactions has a considerably more complex form and can be represented as:

$$f = \frac{A_n + A_{\mu^-} + A_{\mu_f}}{\eta \left[B_n + B_{\mu^-} + B_{\mu_f}\right]} \quad (3)$$

where the parameters A_i and B_i (with i = n, μ^-, or μ_f indicating the neutron spallation, negative muon capture and fast muon interaction production pathways, respectively) are defined as

$$A_i = x_i^{21} \Lambda_i \left(1 - e^{-\frac{\eta}{\Lambda_i} t}\right) \quad (4)$$

$$B_i = \frac{x_i^j}{\lambda_j + \frac{\eta}{\Lambda_i}} \left(1 - e^{-\left(\lambda_j + \frac{\eta}{\Lambda_i}\right) t}\right) \quad (5)$$

Here, x_i^j is the relative contribution of production pathway i to the cosmogenic nuclide with mass number j at the rock surface for the respective sampling location, and Λ_i is the attenuation length for production pathway i.

4.3 Assumptions

As outlined above, for an estimation of the production ratio P_x/P_{21} from factor f and the measured cosmogenic nuclide concentrations the erosion (or mass removal) rate must be known. Total amounts of erosion have been calculated by Goethals et al. (2009) based on a ^{21}Ne production rate of 19 at g^{-1} a^{-1} at sea level and high latitude (Niedermann, 2000). Since our goal is to establish production ratios independently of currently used absolute production rates, we cannot directly convert these values to mass removal rates. However, without any assumption on the production rate it is not possible to limit the possible range of erosion. Therefore, we have allowed for a ±20% range around the 19 at g^{-1} a^{-1} value, which appears as a safe choice that includes the recently published P_{21} values of Amidon et al. (2009) and Balco and Shuster (2009) and should include any other realistic ^{21}Ne production rate value as well. We emphasize that this choice does not lead to a circular argument; we will show in section 5.3 that even for an obviously unrealistic P_{21} assumption the resulting P_{10}/P_{21} and P_{26}/P_{21} do not turn out substantially different. In contrast to Goethals et al. (2009), who assumed that ^{21}Ne production by muons is negligible, here we have incorporated the new finding of Balco and Shuster (2009) that muons contribute ~3.6% to the total P_{21} at sea level and high latitude. These authors state that they cannot

separate this contribution into stopped muon and fast muon fractions. We argue from nuclear systematics that the contribution from negative muon capture is negligible. There are two channels open for particle emission to ^{21}Ne after muon capture in ^{28}Si, (μ^-,3p 4n) or (μ^-,α p 2n), while the production of ^{26}Al requires only the emission of 2 neutrons. Particle emission probabilities shown in Table 1 of Heisinger et al. (2002a) indicate that these channels should be reduced by an order of magnitude or more compared to the 2n channel. We thus conclude that any muon-induced contribution to the ^{21}Ne production rate is due only to fast muon-induced reactions. We therefore adopted the value of 3.6% by Balco and Shuster (2009) for the fast muon contribution as the only measured data available although we would expect a lower value based on the cross sections shown in Table 1 of Heisinger et al. (2002b). The assumption of 3.6% fast muon contribution increases the erosion (or mass removal) rates determined for the different sample sites in the Bishop Tuff by ~5-10% compared to those calculated with no muon contribution (cf. Goethals et al., 2009).

Ranges of 'mass removal' resulting from the assumed ^{21}Ne production rate range are given in Table 4. We deliberately report ranges rather than nominal values with uncertainties, as we do not give preference to any value within this range. Note that these ranges are much wider than those corresponding to the "total erosion" values given in Goethals et al. (2009) because of the additional assumption of a ±20% P_{21} range. Like this, the possible erosion rates vary by a factor of 2 or more for individual samples, instead of a ±10% variation when only the analytical uncertainty of the measurement is taken into account (Goethals et al., 2009). Nevertheless, the effect of even such a large erosion range on the accuracy of the factor f is limited to just a few percent (Table 4, Figure 4).

^{10}Be and ^{26}Al in quartz are mainly formed by spallation reactions of high-energy neutrons on oxygen and silicon, respectively (e.g., Gosse and Phillips, 2001; Niedermann, 2002). To a much lesser extent ^{10}Be and ^{26}Al are also produced by negative muon capture and fast muon interactions, which contribute ~1-4% to the total production at sea level (Brown et al., 1995; Heisinger et al., 1997, 2002a, 2002b). In applying equation 3 we related the muogenic production rates for ^{10}Be given in Heisinger et al. (2002a) to the "reference production rate for spallation" of Balco et al. (2008), assuming that the latter already includes the fast muon production path. For Dunai (2000) scaling, this yields a total P_{10} of 5.01 at g^{-1} a^{-1} at sea level and high latitude, of which 2.1% are caused by negative muon capture and 1.9% by fast muon interactions. For ^{26}Al, the total P_{10} value was multiplied by 6.52 (Kubik et al., 1998), and again the muon production rates of Heisinger et al. (2002a) were related to the resulting 32.6 at g^{-1} a^{-1} production rate, yielding 2.5% and 2.2% contributions by negative and fast muons, respectively. Scaling to the Bishop Tuff latitude (37.42°N) and altitude (1400 m) using the algorithm of Dunai (2000) reduces the negative muon contribution at the rock surface to 1.24% for ^{10}Be and 1.48% for ^{26}Al, due to the different attenuation length in air (247 g/cm^2), while fast muons scale like neutrons (Dunai, 2000). Similar fractions of muogenic production for ^{10}Be and ^{26}Al are also indicated by a similar ^{26}Al/^{10}Be production ratio for muon and spallation reactions; Reedy et al. (1994) report 7.0±0.4 for negative muon capture and Heisinger et al. (2002a) report 7.6±0.9 and 7.7±1.4 for muon capture and fast muons, respectively.

In the literature, effective spallation attenuation lengths for neutron spallation (Λ_n) between approximately 145 and 178 g cm^{-2} have been reported (e.g. Brown et al., 1995; Gosse and Phillips, 2001). Here we use a value of 160 g cm^{-2}, which is most widely adopted. The attenuation lengths for slow and fast muons, 1510 g cm^{-2} and 4320 g cm^{-2} respectively, given in Heisinger et al. (2002a,b) can only be used for rough estimates of the production rate at depth as clearly stated by these authors. An accurate parameterisation of the full depth profile given in Heisinger et al. (2002a,b) can only be achieved by sets of 5 exponential functions. Good fit approximations have been published by e.g. Granger et al. (2001). However, for the depths relevant for our samples (0-4 m) good fits can even be realised with one attenuation length each. For the slow muons we obtain Λ_{μ^-} = 1350 g cm^{-2} and for the fast muons $\Lambda_{\mu f}$ = 2150 g cm^{-2}, which for the fast muons at least is quite different from that of Heisinger et al. (2002b).

4.4 Production rate ratios

Based on the measured nuclide concentrations, the ranges of mass removal rates shown in Table 4, and the other parameters given in section 4.3, we have calculated possible ranges of P_{10}/P_{21} and P_{26}/P_{21} for the 13 studied samples using equation (3) (Table 4, Figure 5). In Figure 5a the results for the 1.39 Ma half-life of ^{10}Be are not shown, as the only difference to the plot for 1.51 Ma would be a systematic downward shift of the ranges by ~0.02 units. The calculation of average values for P_{10}/P_{21} and P_{26}/P_{21} from the ranges derived from individual samples is not quite straightforward because they represent maximum arrays of possible production rate ratios (under the initial assumption that the ^{21}Ne production rate does not deviate more than 20% from 19.0 at g^{-1} a^{-1}) and can thus not be treated in a strictly statistical way. Therefore, we offer two approaches and show that they lead to virtually the same results. The major part of the production ratio range is caused by the (statistically distributed) analytical uncertainties of the cosmogenic nuclide concentrations (see section 5.3). Therefore, for a first approach we use the midpoint values of the ranges and calculate arithmetic means from all samples. For P_{10}/P_{21}, arithmetic means of 0.2494±0.0091 for the 1.51 Ma half-life and 0.2320±0.0084 for the 1.39 Ma half-life are obtained, for P_{26}/P_{21} the arithmetic mean is 1.812±0.076. Here, the uncertainties (given as two standard

deviations of the mean) may underestimate the real error limits on those production ratios because the uncertainties of the individual values are not taken into account. On the other hand, it is possible to calculate error-weighted means, where half the extent of the production ratio range is taken as the error. This second approach yields P_{10}/P_{21} of 0.2481±0.0081 (^{10}Be half-life of 1.51 Ma) and 0.2308±0.0076 (^{10}Be half-life of 1.39 Ma), respectively, and P_{26}/P_{21} of 1.795±0.084. In this case the uncertainties might overestimate the production ratio uncertainties, because the maximum ranges were incorrectly treated as statistical error limits. However, both methods yield essentially identical mean values and error limits, confirming that the variation among the sample set is essentially only due to the analytical uncertainties of the cosmogenic nuclide concentrations and does not contain a major systematic component. We therefore propose conservative estimates of 0.249±0.009 (^{10}Be half-life 1.51 Ma) or 0.232±0.009 (^{10}Be half-life 1.39 Ma) for P_{10}/P_{21} and 1.80±0.09 for P_{26}/P_{21}, respectively (Table 5).

5. Discussion

5.1 Comparison of new production ratios to literature data

Our proposed P_{10}/P_{21} ratio of 0.249±0.009 based on the 1.51 Ma half-life can be compared to that obtained for a set of samples from the Sierra Nevada (Nishiizumi et al., 1989; Niedermann et al., 1994). In these relatively young samples (~13 ka; Clark et al., 1995) with negligible erosion, radioactive decay of ^{10}Be is insignificant and therefore P_{10}/P_{21} equals C_{10}/C_{21}. The two samples analysed for both ^{10}Be and ^{21}Ne yield $P_{10}/P_{21} \leq$ (0.214±0.081) (W86-12) and $P_{10}/P_{21} \geq$ (0.271±0.064) (W86-8). Note that to calculate these ratios, the ^{10}Be concentrations originally reported by Nishiizumi et al. (1989) have been multiplied by a factor of 0.987. Like this, they can directly be compared with our Be data, which were measured at ETH Zurich using a different standard normalization and a slightly different half-life (1.5 versus 1.51 Ma) (Kubik and Christl, subm. manuscript). The fact that only upper and lower limits, respectively, can be given for the Sierra Nevada samples is due to the difficult corrections for non-cosmogenic ^{21}Ne (Niedermann et al., 1994). The upper and lower limits are, however, consistent within their uncertainty ranges and yield a common P_{10}/P_{21} of 0.251±0.044, very similar to the value obtained above from the Bishop Tuff samples, but much less precise. ^{10}Be/^{21}Ne production ratios have recently also been reported by Balco and Shuster (2009) and Amidon et al. (2009), normalised to a ^{10}Be half-life of 1.36 Ma (Nishiizumi et al., 2007). Their values of 0.245±0.022 and 0.275±0.025, respectively, are slightly to considerably higher than our result for the 1.39 Ma half-life (0.232±0.009).

Our P_{26}/P_{21} value of 1.80±0.09 can again be compared to that obtained in the quartz samples from the Sierra Nevada, which is lower at 1.65±0.28 (Niedermann et al., 1994); note that the ^{26}Al concentrations given by Nishiizumi et al. (1989) – which were used by Niedermann et al. (1994) for calculating the ^{26}Al/^{21}Ne production ratio – were multiplied by 1.072 (Kubik and Christl, subm. manuscript) to be directly comparable with our data. Likewise, Balco and Shuster (2009) have reported a P_{26}/P_{21} of 1.65±0.15. These values are thus consistent within 2σ error limits with our new P_{26}/P_{21}, which has however a smaller uncertainty.

The production ratio of ^{26}Al/^{10}Be has been studied more frequently; published values vary between ~6 and ~7. For young samples (<100 ka), ^{26}Al/^{10}Be concentration ratios correspond to production ratios because radioactive decay is negligible. The early work by Nishiizumi et al. (1989) indicated a P_{26}/P_{10} of 6.02±0.44 (1σ error). Taking into account the different half-lives and AMS standard normalizations used by those authors, this value must be multiplied by a factor of 1.086 and converts to 6.54±0.48 for the ^{10}Be half-life of 1.51 Ma (Kubik and Christl., subm. manuscript). Kubik et al. (1998) determined a mean value of 6.52±0.43 (1σ error) from four samples of the Köfels landslide, Austria, using the same normalizations as in this study, hence no correction is needed. The adopted normalization correction thus leads to an excellent agreement between the Nishiizumi et al. (1989) and Kubik et al. (1998) studies. Clapp et al. (2001) report a ^{26}Al/^{10}Be concentration ratio of 6.52±0.31 (1σ error). Corrected for AMS standard and half-lives, this ratio increases to 7.08±0.67 (2σ error). When we use the Bishop Tuff values for P_{10}/P_{21} and P_{26}/P_{21} to calculate P_{26}/P_{10}, we obtain a ratio that is somewhat higher still: 7.23±0.45 when normalized to the 1.51 Ma ^{10}Be half-life, or 7.76±0.49 for the 1.39 Ma half-life (Table 5).

5.2 Potential reasons for the relatively high ^{26}Al/^{10}Be production ratio in comparison to previous determinations

Our P_{26}/P_{10} value of 7.23±0.45 for the 1.51 Ma ^{10}Be half-life is higher than those determined earlier by Nishiizumi et al. (1989) and Kubik et al. (1998), even though they all agree within 2σ error limits. There are several possible reasons for the unsatisfactory agreement. For example, a high ratio might result from either too low ^{10}Be or too high ^{26}Al concentrations in our samples. If the Bishop Tuff quartz contained sizeable amounts of native ^{9}Be, then the Be concentration in the AMS target, usually given by that of the Be carrier alone, could have been underestimated. To decrease the measured ^{10}Be concentration by ~10-20%, as would be suggested from the high ^{26}Al/^{10}Be ratios, would require a native Be content of ~0.06-0.08 mg in addition to the Be carrier through which ~0.3-0.4 mg Be were added. However, a test with 10 aliquots from purified quartz samples resulted in an average of only 0.0010 mg Be in ~10 gram quartz (i.e. 0.1 ppm). In all these samples the amount of natural Be was less than 1% of the Be carrier. Therefore, the natural Be in the samples did not affect the P_{26}/P_{10}.

Other sources of error for the ^{10}Be analysis may be the lack of equilibration of carrier and sample during chemical processing (regarded unlikely due to good reproducibility), the fractionation of ^{10}Be against ^{9}Be during chromatographic separation (regarded unlikely) and a wrong carrier calibration. However, the Bishop Tuff samples were measured using two different ^{9}Be carrier solutions, and there is no indication that the carriers biased the Be results (Table 3).

The second possibility is an overestimation of ^{26}Al in our samples in connection with the ICP-OES analysis of stable Al (section 3.5). For example, if the concentration of stable Al would have been overestimated by ~10% for our samples, the real P_{26}/P_{10} would be ~10% lower, yielding agreement with previously published values. Hence, we performed our Al measurements using the standard addition technique, which avoids matrix effects. Because our Al concentrations were higher than we expected based on previously published P_{26}/P_{10}, an independent duplicate analysis was performed (section 3.5). The duplicate analysis (ICP-analyte concentration ~3-9 ppm, 396 nm wavelength) resulted in values similar to the initial results (ICP-analyte concentrations 0.3-2 ppm, 167 nm wavelength; Table 2). Furthermore, a rock standard analysed with the same analytical method yielded an accurate Al concentration (section 3.5). Thus, we are confident that our data are robust and that the high P_{26}/P_{10} production rate ratio is not due to an overestimated stable aluminium concentration.
An alternative explanation is that Al concentrations were underestimated in previously published studies. There are several possibilities for such discrepancies. For example, the Al concentrations obtained with the ordinary calibration curve analysis on the duplicates were 7-11% lower than those obtained by standard addition. This discrepancy points to the importance of matrix effects on the measured Al concentration (Table 2). An underestimation of Al can also be caused by incomplete recovery of Al from the HF sample solutions (Bierman and Caffee, 2002). Other, although less likely causes, include loss of Al by a fractionation of ^{27}Al against ^{26}Al on the chromatography column if column yields are low, or loss during sample processing, possibly as $Al(NO_3)_3 \times 9\ H_2O$, because of the relatively low boiling point of this compound of 150°C (Weast, 1974). With respect to the latter we note that the temperatures of our sample solutions during Al and Be extraction never exceeded 120°C. Thus, there are a number of possible reasons for underestimating Al concentrations and thus the P_{26}/P_{10} production ratio.

5.3 Effects of uncertainties in erosion rate, muon contributions and attenuation lengths and of the applied scaling procedure on derived production ratios

We assessed the potential ranges of erosion experienced by each sample by assuming that the ^{21}Ne production rate deviates at most 20% from the value reported by Niedermann (2000). This assumption might be suspected to bias the results in such a way that the returned production rate ratios are adjusted to the assumed ^{21}Ne production rate; however, this is clearly not the case. In spite of the large ranges of erosion compatible with the assumed ^{21}Ne production rate range (Table 4), the effect on the production ratios is only ~±2% and ~±3% for P_{10}/P_{21} and P_{26}/P_{21}, respectively, if the analytical uncertainties of the cosmogenic nuclide concentrations are not taken into account. Their effect is much larger, on average ~15% for both ratios. Even when an obviously unrealistic assumption for the ^{21}Ne production rate is used to estimate the erosion rates, such as 30 atoms g^{-1} a^{-1} (i.e., 58% higher than the value of Niedermann, 2000), the resulting production rate ratios are only slightly affected: ~4% lower for P_{10}/P_{21} and ~6% lower for P_{26}/P_{21}. This shows that the initial assumption about P_{21} is safe and does not bias the results for P_x/P_{21}.
Besides the uncertainties of the erosion rate, also the other assumptions that were made in the calculations, such as the contributions by muon interactions or the attenuation lengths, have an influence on the determined production ratios. In principle, a distinct difference in muon production contributions for ^{10}Be and ^{26}Al could contribute to the relatively high ^{26}Al/^{10}Be production rate ratio. However, the effect would be small in relation to the production induced by spallation. The samples that we took at the present-day surface of the Bishop Tuff were initially at depths of 100-300 cm and have been exhumed by erosion (Goethals et al., 2009). Due to the higher attenuation length of muons in rock (>1300 g cm^{-2}; see section 4.3) compared to neutrons (~160 g cm^{-2}), the production by muons at depth decreases less rapidly than the production by neutron spallation. Nevertheless, even at 3 m depth the muon contribution to total production is <40% at the Bishop Tuff location (elevation ~1400 m, rock density 1.65 g/cm^3), and a clear difference in P_{26}/P_{10} between spallation and muon-induced reactions would be needed to give a sizeable effect on the total ratio. Completely neglecting any muon-induced contribution to ^{10}Be, ^{21}Ne and ^{26}Al production (i.e., using equation 2 instead of 3), the P_{10}/P_{21} and P_{26}/P_{21} production rate ratios would decrease by only ~0.8% and ~0.4%, respectively, and changing the assumptions for the contributions of the different production pathways (x_i^j in equations 4 and 5) within reasonable limits would result in similarly small differences.
We assumed an effective attenuation length of 160 g cm^{-2} for cosmic-ray neutron spallation reactions in rock, which is not very well constrained (section 4.3). It could be expected that this uncertainty might severely affect the results. However, the effect of a change in attenuation length is indeed very small, because in both the equation used to derive the erosion rate (Goethals et al., 2009) and that for the factor f (equation 3) the neutron

attenuation length and the erosion rate always appear as their combined ratio, except for the terms describing the muon contributions. In other words, increasing the attenuation length will reduce the calculated erosion rate in such a way that their ratio remains the same, and the factor f is only marginally changed due to the muon production terms. For example, changing the spallation attenuation length to 180 g cm^{-2} would increase the resulting production rate ratios by only ~0.02%. Therefore, the choice of the spallation attenuation length barely affects the results. And although the muon attenuation lengths are even less well constrained than the one for neutron-induced spallation, the overall effect of the muon terms on the resulting production ratios is so small that the influence of the chosen muon attenuation lengths is clearly insignificant.

Scaling for altitude and latitude came into play at two steps in our procedure. First, the erosion ranges for each sample (Table 4) were estimated assuming a P_{21} of 19.0 at g^{-1} a^{-1} (±20%), which is the value derived from the production rate calibration of Niedermann et al. (1994) by scaling to sea level and high latitude using Dunai (2000). Other scaling methods, such as Lal (1991), Stone (2000) or Desilets et al. (2006), yield normalized P_{21} values deviating by at most 7% from that value, i.e. well within the 20% range that we allowed for. In addition, as the Bishop Tuff is located geographically very close to the Sierra Nevada P_{21} calibration site of Niedermann et al. (1994), part of the scaling offset will cancel when scaling back to the Bishop Tuff site, and as discussed above even substantially different assumptions for P_{21} would only have a small effect on the resulting P_{10}/P_{21} and P_{26}/P_{21} values. The second point where scaling is involved is the stopped muon contribution to total production (x_{μ}^{j} in equation 3) at the Bishop Tuff site. Applying a different scaling scheme might slightly change this value; however since the influence of the assumed muon contribution on the final production ratio values is small anyway, the scaling issue can be neglected in this context. In summary, our P_{10}/P_{21} and P_{26}/P_{21} values are essentially independent of the scaling method.

6. Conclusions

Measurements of the cosmogenic nuclides ^{21}Ne, ^{10}Be, and ^{26}Al in samples from the Bishop Tuff, California, allowed us to determine a $^{10}Be/^{21}Ne$ production ratio in quartz of 0.249±0.009 (for a ^{10}Be half life of 1.51 Ma) or 0.232±0.009 (for a ^{10}Be half-life of 1.39 Ma) and an $^{26}Al/^{21}Ne$ production ratio of 1.80±0.09, respectively. When combined with the relatively well-established production rate of ^{10}Be of 5.01 at g^{-1} a^{-1} at sea level and high latitude (Balco et al., 2008 with an additional 2.1% muon capture contribution), which holds for Dunai (2000) scaling and the 1.51 Ma ^{10}Be half-life, our accurate production ratios yield absolute production rates for cosmogenic ^{21}Ne and ^{26}Al of 20.1 and 36.2 at g^{-1} a^{-1}, respectively (Table 5). Using the most recent ^{10}Be half-life determinations of 1.39 Ma instead (Chmeleff et al., 2009; Korschinek et al., 2009), the total ^{10}Be production rate decreases to 4.61 at g^{-1} a^{-1}, while the production rates of ^{21}Ne and ^{26}Al are only slightly changed to 19.9 and 35.7 at g^{-1} a^{-1}, respectively (Table 5). As our production ratios are essentially independent of the scaling method used, absolute production rates valid for other scaling methods than Dunai (2000) can be calculated easily from the respective ^{10}Be production rate (e.g. Balco et al., 2008).

Acknowledgements

This research was funded as part of the EU Marie-Curie Research and Training Network "CRONUS-EU" (RTN project reference 511927) and was additionally supported by Deutsches GeoForschungsZentrum Potsdam. We would like to acknowledge J. Glodny, K. Hahne, R. Naumann, E. Schnabel and S. Tonn (Potsdam); J. Berndt-Gerdes, N. Gussone and K. Mezger (Münster); D. Merten (Jena); F. Kober and S. Ivy-Ochs (Zurich) and P. Vermeesch (London) for sample preparation, analyses and helpful discussions. We thank Rainer Wieler and an anonymous reviewer for constructive comments that have helped to improve the manuscript.

References

Amidon, W.H., Rood, D.H., Farley, K.A., 2009. Cosmogenic ^{3}He and ^{21}Ne production rates calibrated against ^{10}Be in minerals from the Coso volcanic field. Earth and Planetary Science Letters 280, 194-204.

Balco, G., Shuster, D.L., 2009. Production rate of cosmogenic ^{21}Ne in quartz estimated from ^{10}Be, ^{26}Al, and ^{21}Ne concentrations in slowly eroding Antarctic bedrock surfaces. Earth and Planetary Science Letters 281, 48-58.

Balco, G., Stone, J.O., Lifton, N.A., Dunai, T.J., 2008. A complete and easily accessible means of calculating surface exposure ages or erosion rates from ^{10}Be and ^{26}Al measurements. Quaternary Geochronology 3, 174-195.

Bennett, E.R., Youngson, J.H., Jackson, J.A., Norris, R.J., Raisbeck, G.M., Yiou, F., Fielding, E., 2005. Growth of south rough ridge, Central Otago, New Zealand: Using in situ cosmogenic isotopes and geomorphology to study an active blind reverse fault. Journal of Geophysical Research 110, B02404, doi: 10.1029/2004JB003184.

Bierman, P.R., Caffee, M., 2002. Cosmogenic exposure and erosion history of Australian bedrock landforms. Geological Society of America Bulletin 114, 787-803.

Brown, E.T., Bourlès, D.L., Colin, F., Raisbeck, G.M., Yiou, F., Desgarceaux, S., 1995. Evidence for muon-induced production of ^{10}Be in near-surface rocks from the Congo. Geophysical Research Letters 22, 703-706.

Chmeleff, J., von Blanckenburg, F., Kossert, K., Jakob, D., 2009. Determination of the ^{10}Be half-life by Multi Collector ICP-Mass Spectrometry and Liquid Scintillation Counting. Goldschmidt Conference Davos, Geochimica et Cosmochimica Acta, in press.

Clapp, E.M., Bierman, P.R., Nichols, K.K., 2001. Rates of sediment supply to arroyos from upland erosion determined using *in situ* produced cosmogenic ^{10}Be and ^{26}Al. Quaternary Research 55, 235-245.

Clark, D.H., Bierman, P.R., Larsen, P., 1995. Improving in situ cosmogenic chronometers. Quaternary Research 44, 367-377.

Desilets, D., Zreda, M., Prabu, T., 2006. Extended scaling factors for in situ cosmogenic nuclides: New measurements at low latitude. Earth and Planetary Science Letters 246, 265-276.

Dunai, T.J., 2000. Scaling factors for production rates of in situ produced cosmogenic nuclides: a critical reevaluation. Earth and Planetary Science Letters 176, 157-169.

Fink, D., Smith, A., 2007. An intercomparison of ^{10}Be and ^{26}Al AMS reference standards and the ^{10}Be half-life. Nuclear Instruments and Methods in Physics Research B 259, 600-609.

Goethals, M.M., Niedermann, S., Hetzel, R., Fenton, C.R., 2009. Determining the impact of faulting on the rate of erosion in a low-relief landscape: A case study using *in situ* produced ^{21}Ne on active normal faults in the Bishop Tuff, California. Geomorphology 103, 401-413.

Gosse, J.C., Phillips, F.M., 2001. Terrestrial in situ cosmogenic nuclides: theory and application. Quaternary Science Reviews 20, 1475-1560.

Govindaraju, K., 1980. Report (1980) on three GIT-IWG rock reference samples: Anorthosite from Greenland, AN-G, basalte d'Essey-la-Côte, B $\times 10^{-N}$, granite de Beauvoir, MA-N. Geostandards Newsletter 4, 49-138.

Govindaraju, K., Roelandts, I., 1993. Second report (1993) on the first three GIT-IWG rock reference samples: Anorthosite from Greenland, AN-G; Basalte d'Essey-la Côte, B $\times 10^{-N}$; Granite de Beauvoir, MA-N. Geostandards Newsletter 172, 227-294.

Granger, D.E., 2006. A review of burial dating methods using ^{26}Al and ^{10}Be, in: Siame, L.L., Bourlès, D.L., and Brown, E.T., (eds)., In Situ-Produced Cosmogenic Nuclides and Quantification of Geological Processes: Geological Society of America Special Paper 415, p. 1-16.

Granger, D.E., Smith, A.L., 2000. Dating buried sediments using radioactive decay and muogenic production of ^{26}Al and ^{10}Be. Nuclear Instruments and Methods in Physics Research B 172, 822-826.

Granger, D.E., Riebe, C.S., Kirchner, J.W. Finkel, R.C., 2001. Modulation of erosion on steep granitic slopes by boulder armouring, as revealed by cosmogenic ^{26}Al and ^{10}Be. Earth and Planetary Science Letters 186, 269-281.

Heisinger, B., Niedermayer, M., Hartmann, F.J., Korschinek, G., Nolte, E., Morteani, G., Neumaier, S., Petitjean, C., Kubik, P., Synal, A., Ivy-Ochs, S., 1997. In-situ production of radionuclides at great depths. Nuclear Instruments and Methods in Physics Research B 123, 341-346.

Heisinger, B., Lal, D., Jull, A.J.T., Kubik, P., Ivy-Ochs, S., Knie, K., Nolte, E., 2002a. Production of selected cosmogenic radionuclides by muons: 2. Capture of negative muons. Earth and Planetary Science Letters 200, 357-369.

Heisinger, B., Lal, D., Jull, A.J.T., Kubik, P., Ivy-Ochs, S., Neumaier, S., Knie, K., Lazarev, V., Nolte, E., 2002b. Production of selected cosmogenic radionuclides by muons: 1. Fast muons. Earth and Planetary Science Letters 200, 345-355.

Hetzel, R., Niedermann, S., Ivy-Ochs, S., Kubik, P.W., Tao, M., Gao, B., 2002. ^{21}Ne versus ^{10}Be and ^{26}Al exposure ages of fluvial terraces: the influence of crustal Ne in quartz. Earth and Planetary Science Letters 201, 575-591.

Hofmann, H.J., Beer, J., Bonani, G., Von Gunten, H.R., Raman, S., Suter, M., Walker, R.L., Wölfli, W., Zimmermann, D., 1987. ^{10}Be half-life and AMS-standards. Nuclear Instruments and Methods in Physics Research B 29, 32-36.

Jennings, S.A., Elliott-Fisk, D.L., 1993. Packrat midden evidence of late Quaternary vegetation change in the White Mountains, California-Nevada. Quaternary Research 39, 214-221.

Kohl, C.P., Nishiizumi, K., 1992. Chemical isolation of quartz for measurement of *in-situ*-produced cosmogenic nuclides. Geochimica et Cosmochimica Acta 56, 3583-3587.

Korschinek, G., Bergmaier, A., Dillmann, I., Faestermann, T., Gerstmann, U., Knie, K., von Gostomski, C.L., Maiti, M., Poutivtsev, M., Remmert, A., Rugel, G., Wallner, A., 2009. Determination of the ^{10}Be half-life by HI-ERD and Liquid Scintillation Counting. Goldschmidt Conference Davos, Geochimica et Cosmochimica Acta, in press.

Kubik, P.W., Christl, M., subm. manuscript 2009. ^{10}Be and ^{26}Al measurements at the Zurich 6 MV Tandem AMS facility. Nuclear Instruments and Methods in Physics Research B.

Kubik, P.W., Ivy-Ochs, S., Masarik, J., Frank, M., Schlüchter, C., 1998. ^{10}Be and ^{26}Al production rates deduced from an instantaneous event within the dendro-calibration curve, the landslide of Köfels, Ötz Valley, Austria. Earth and Planetary Science Letters 161, 231-241.

Lal, D., 1991. Cosmic ray labeling of erosion surfaces: in situ nuclide production rates and erosion models. Earth and Planetary Science Letters 104, 424-439.

Licciardi, J.M., Kurz, M.D., Curtice, J.M., 2006. Cosmogenic ^{3}He production rates from Holocene lava flows in Iceland. Earth and Planetary Science Letters 246, 251-264.

Ludwig, K.R., 2003. User's manual for a geochronological toolkit for Microsoft Excel. Berkeley Geochronology Center Special Publication, No 4.

Niedermann, S., 2000. The ^{21}Ne production rate in quartz revisited. Earth and Planetary Science Letters 183, 361-364.

Niedermann, S., 2002. Cosmic-ray produced noble gases in terrestrial rocks: dating tools for surface processes. In: Porcelli, D., Ballentine, C.J., Wieler, R., (Eds.), Noble Gases in Geochemistry and Cosmochemistry, Reviews in Mineralogy and Geochemistry 47, 731-784.

Niedermann, S., Graf, T., Kim, J.S., Kohl, C.P., Marti, K., Nishiizumi, K., 1994. Cosmic-ray-produced ^{21}Ne in terrestrial quartz: the neon inventory of Sierra Nevada quartz separates. Earth and Planetary Science Letters 125, 341-355.

Niedermann, S., Bach, W., Erzinger, J., 1997. Noble gas evidence for a lower mantle component in MORBs from the southern East Pacific Rise: Decoupling of helium and neon isotope systematics. Geochimica et Cosmochimica Acta 61, 2697-2715.

Nishiizumi, K., Winterer, E.L., Kohl, C.P., Klein, J., Middleton, R., Lal, D., Arnold, J.R., 1989. Cosmic ray production rates of ^{10}Be and ^{26}Al in quartz from glacially polished rocks. Journal of Geophysical Research 94, 17,907-17,915.

Nishiizumi, K., Imamura, M., Caffee, M.W., Southon, J.R., Finkel, R.C., McAninch, J., 2007. Absolute calibration of ^{10}Be AMS standards. Nuclear Instruments and Method in Physics Research B 258, 403-413.

Ochs, M., Ivy-Ochs, S., 1997. The chemical behaviour of Be, Al, Fe, Ca and Mg during AMS target preparation from terrestrial silicates modelled with chemical speciation calculations. Nuclear Instruments and Method in Physics Research B 123, 235-240.

Plug, L.J., Gosse, J.C., McIntosh, J.J., Bigley, R., 2007. Attenuation of cosmic ray flux in temperate forest. Journal of Geophysical Research 112, F02022, doi:10.1029/2006JF000668.

Reedy, R.C., Nishiizumi, K., Lal, D., Arnold, J.R., Englert, P.A.J., Klein, J., Middleton, R., Jull, A.J.T., Donahue, D.J., 1994. Simulations of terrestrial in-situ cosmogenic production. Nuclear Instruments and Method in Physics Research B 92, 297-300.

Sarafin, S., 1985. Anwendung radiochemischer Methoden und der Beschleuniger-Massenspektrometrie zur Bestimmung der tiefenabhängigen, langlebigen Spallations-Radionuklide ^{10}Be, ^{26}Al, ^{36}Cl und ^{53}Mn in Steinmeteoriten und Gedanken zum ungeklärten Ursprung der Shergottite, Dissertation, Universität zu Köln, Germany.

Sarna-Wojcicki, A.M., Pringle, M.S., Wijbrans, J., 2000. New ^{40}Ar/^{39}Ar age of the Bishop Tuff from multiple sites and sediment rate calibration for the Matuyama-Brunhes boundary. Journal of Geophysical Research 105, 21,431-21,443.

Schulz, O., Heitland, P., 2001. Application of prominent spectral lines in the 125-180 nm range for inductively coupled plasma optical emission spectrometry. Fresenius Journal of Analytical Chemistry 371, 1070-1075, doi: 10.1007/s002160100993

Stone, J.O., 2000. Air pressure and cosmogenic isotope production. Journal of Geophysical Research 105, 23,753-23,759.

van den Bogaard, P., Schirnick, C., 1995. ^{40}Ar/^{39}Ar laser probe ages of Bishop Tuff quartz phenocrysts substantiate long-lived silicic magma chamber at Long Valley, United States. Geology 23, 759-762.

Vermeesch, P., 2007. CosmoCalc: an Excel add-in for cosmogenic nuclide calculations: Geochemistry, Geophysics, and Geosystems 8, Q08003, doi: 10.1029/2006GC001530

Weast, R.C., 1974. Handbook of Chemistry and Physics, CRC Press, Ohio, USA.

Wilson, C.J.N., Hildreth, W., 1997. The Bishop Tuff: New Insights from Eruptive Stratigraphy. The Journal of Geology 105, 407-439.

Wilson, C.J.N., Hildreth, W., 2003. Assembling an ignimbrite: Mechanical and thermal building blocks in the Bishop Tuff, California. The Journal of Geology 111, 653-670.

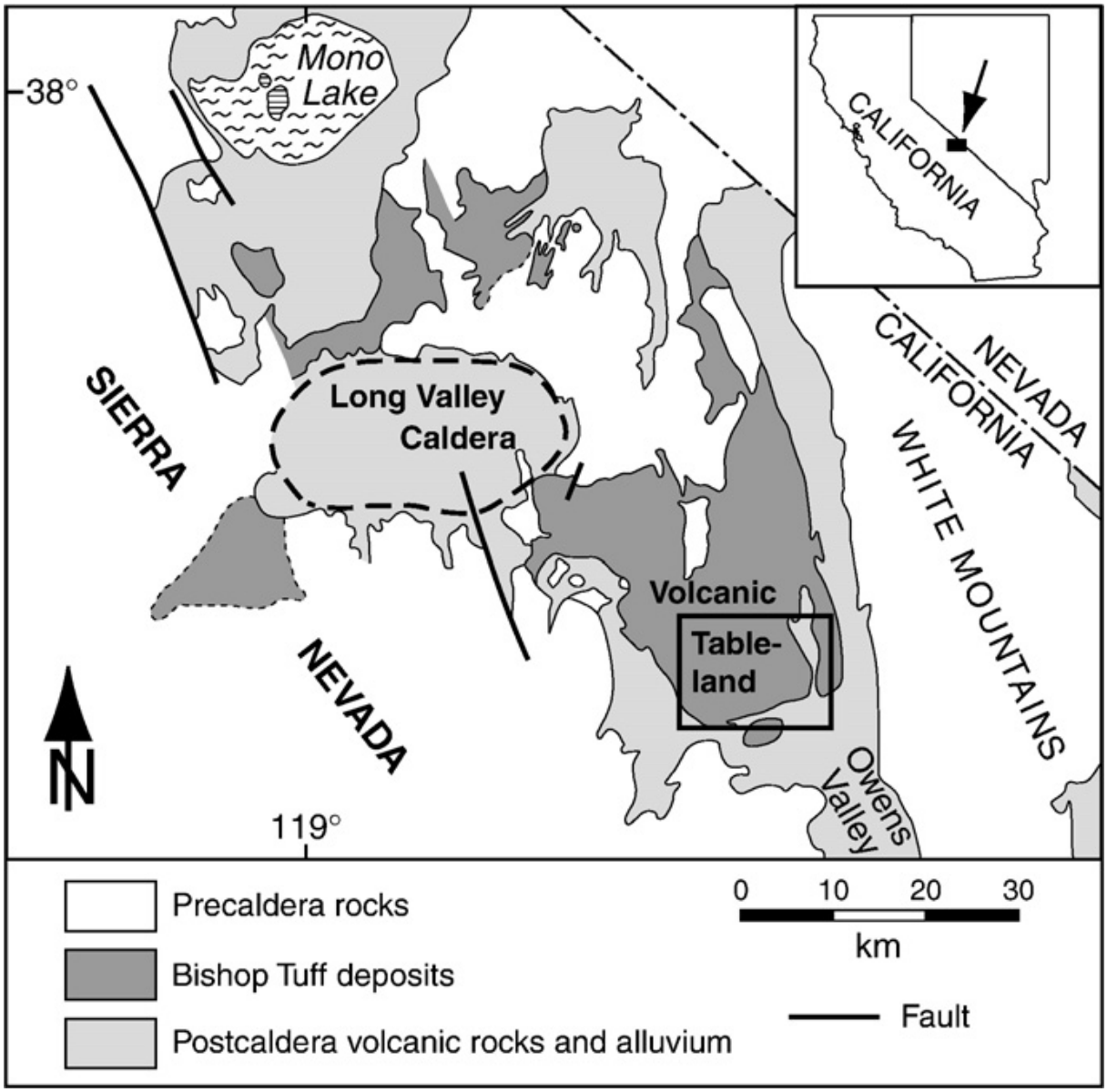

Figure 1: Map showing the location of the Bishop Tuff in eastern California (modified from Sarna-Wojcicki et al., 2000). The black rectangle indicates the Volcanic Tableland where samples for this study were taken. For more detailed maps refer to Goethals et al. (2009).

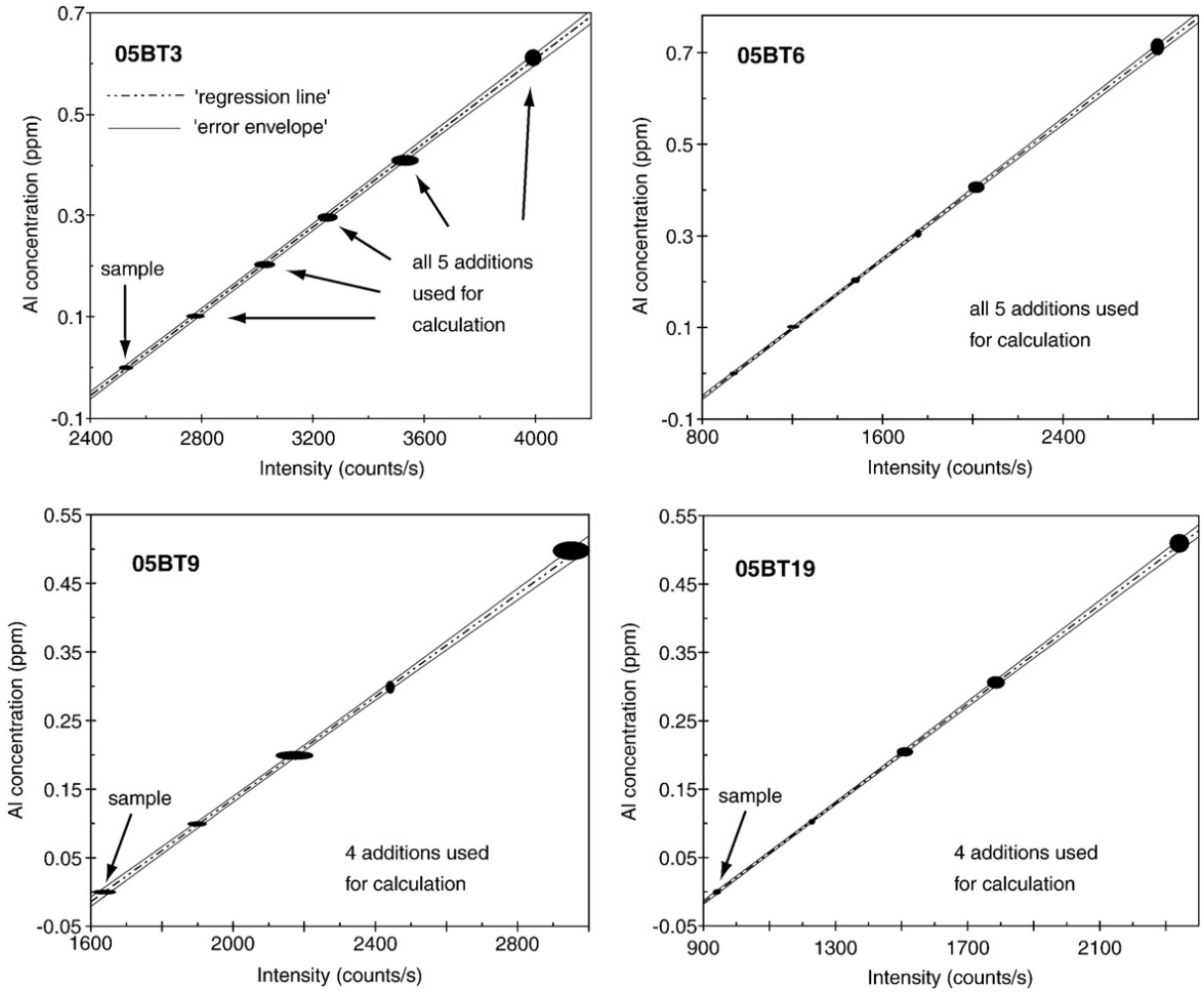

Figure 2: Standard addition plots for four Bishop Tuff samples. Al additions are indicated by error ellipses, whereas 'sample' refers to the sample solution to which no Al was added. The y-axis shows the added concentration of the standard, which is known. The Al concentration in the sample corresponds to the negative intercept of the regression line with the y-axis; note that intercepts are not shown as they lie far to the left. Plots are modified from Isoplot3 results (Ludwig, 2003). See section 3.5 for further explanation.

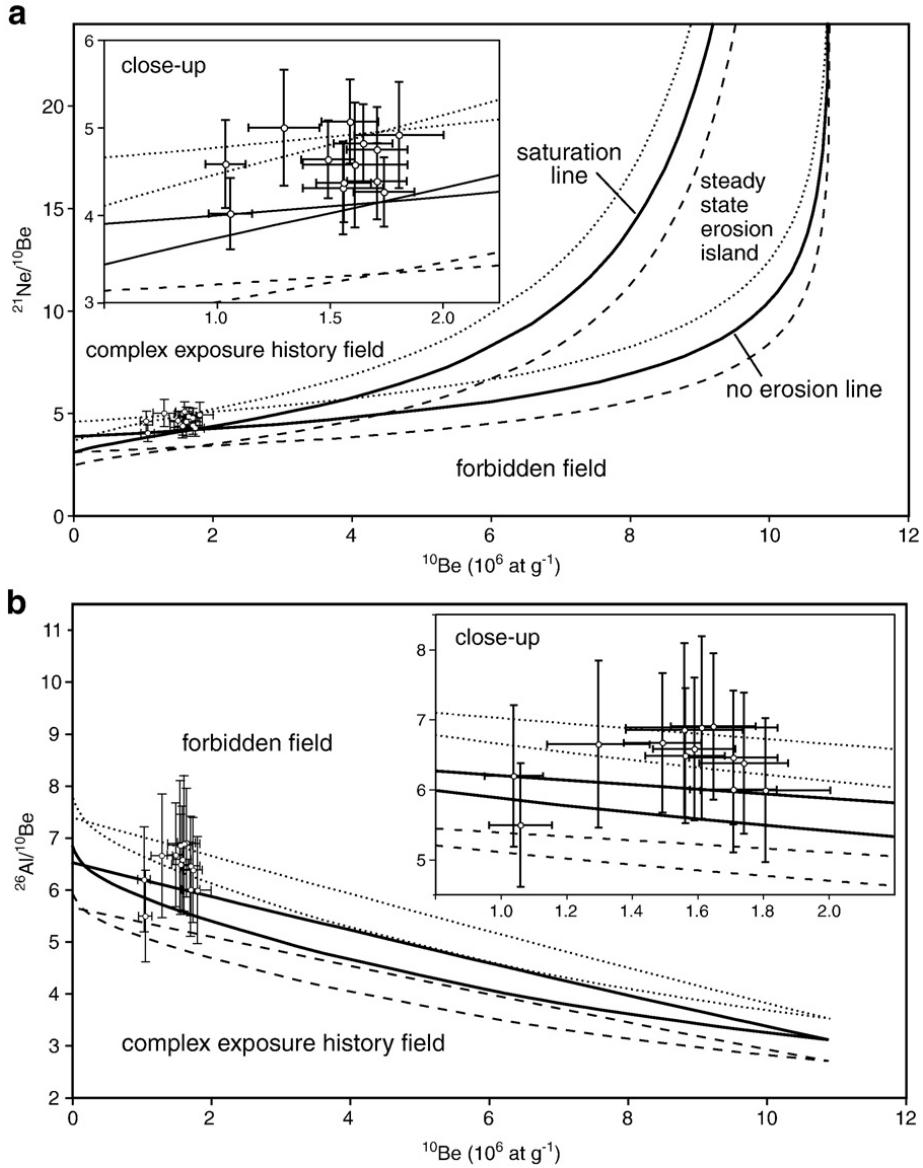

Figure 3: Erosion island plots for the Bishop Tuff samples, shown with linear axes. Error bars represent 2σ. **(a)** Plot of $^{21}Ne/^{10}Be$ versus ^{10}Be. **(b)** Plot of $^{26}Al/^{10}Be$ versus ^{10}Be. Plots are modified from CosmoCalc output (Vermeesch, 2007) using the following parameters to construct the plots: decay constants of 4.59×10^{-7} a^{-1} for ^{10}Be and 9.63×10^{-7} a^{-1} for ^{26}Al, scaling according to Dunai (2000), a rock density of 1.65 g cm^{-3}, and the CosmoCalc settings for the muon production contribution of ^{10}Be and ^{26}Al, based on the approach of Granger and Smith (2000) and Granger et al. (2001). Assumed production rates for the plots shown in solid black lines are 5.01, 19.0, and 32.6 at g^{-1} a^{-1} for ^{10}Be, ^{21}Ne, and ^{26}Al, respectively. Dotted lines represent the upper error limits (i.e., using ^{21}Ne and ^{26}Al production rates of 22.7 and 36.9 at g^{-1} a^{-1}, respectively), and dashed lines represent the lower error limits (15.3 and 28.3 at g^{-1} a^{-1}, respectively). The insets show enlarged views of the areas where the Bishop Tuff samples plot.

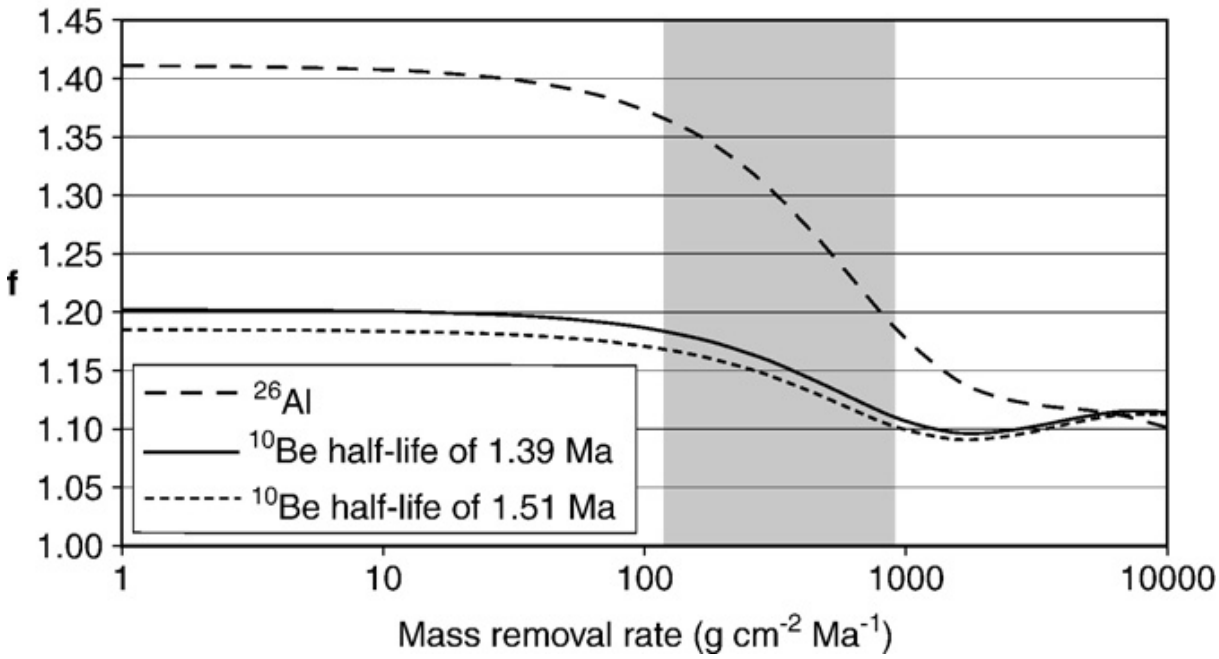

Figure 4: Diagram illustrating the dependence of the factor f (as defined by equation 1) on the mass removal rate for the 760 ka old surface of the Bishop Tuff. The representation including muon-induced production pathways (equation 3) was used, with Λ_i and x_i^j as given in section 4.3. For ^{10}Be, curves for two half-lives of 1.51 and 1.39 Ma (λ_{10} = 0.459 and 0.499 Ma^{-1}, respectively) are shown; the ^{26}Al curve is for a 0.72 Ma half-life (λ_{26} = 0.963 Ma^{-1}). The shape of the curves at very high mass removal rates (>1000 g cm^{-2} Ma^{-1}) depends critically on the assumptions for neutron and muon production contributions. The grey shading indicates the maximum range of mass removal rates potentially experienced by our samples (Table 4), based on the assumption that the ^{21}Ne production rate may deviate by ±20% from the value reported by Niedermann (2000). Note that the factor f depends only weakly on the mass removal rate; e.g. a difference by a factor of 2 in the mass removal rate results in only a few percent difference in f. Note the logarithmic x-axis.

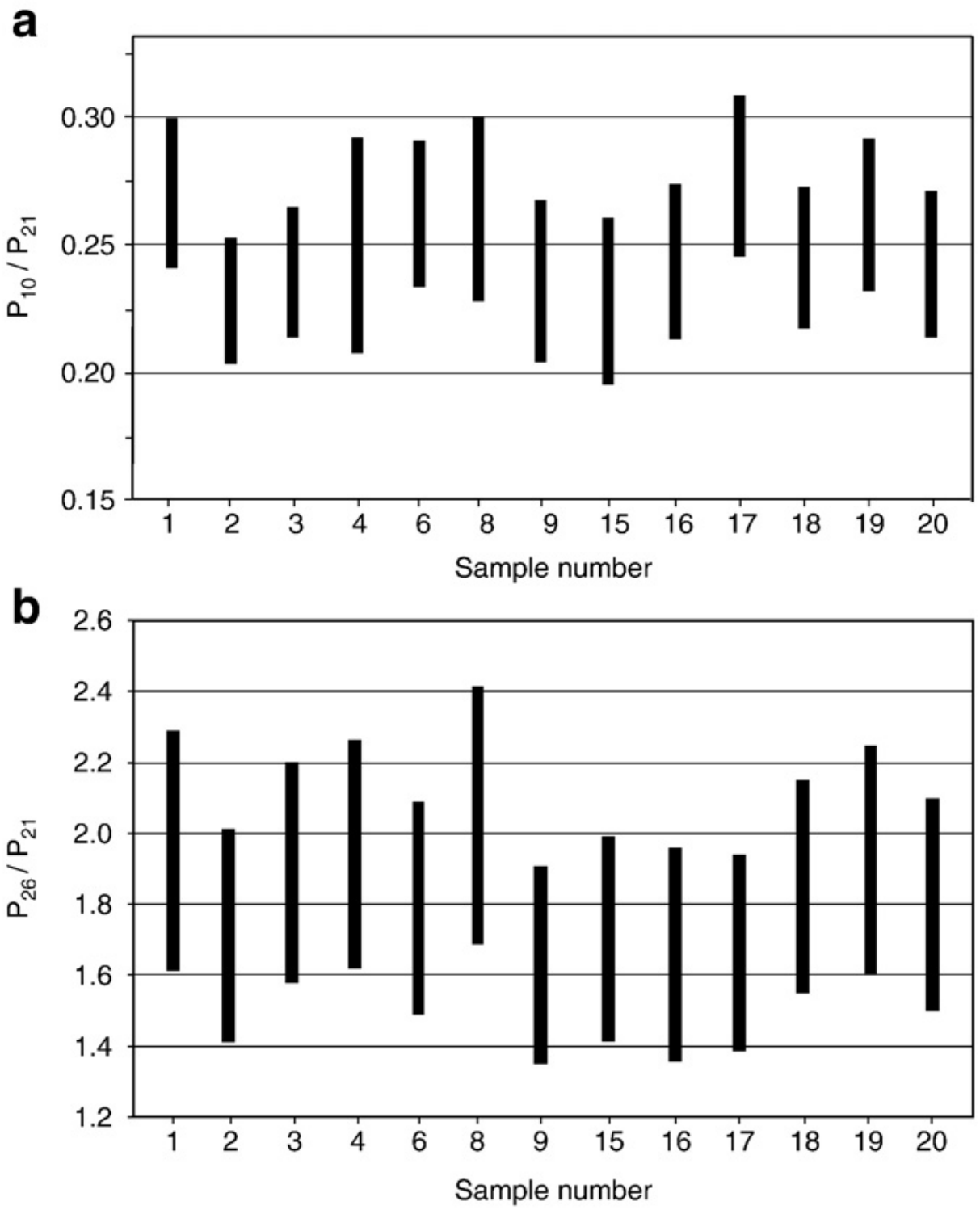

Figure 5: Ranges of production rate ratios P_{10}/P_{21} (for a ^{10}Be half life of 1.51 Ma) and P_{26}/P_{21} as obtained from 13 Bishop Tuff samples. Sample number x refers to 05BTx.

Table 1: Location and description of samples from the Volcanic Tableland, Bishop Tuff, California

Sample ID	Sample type	Latitude (°N)	Longitude (°W)	Elevation (m)
05BT1	bedrock	37.4566	118.4877	1507
05BT2	bedrock	37.4499	118.4884	1502
05BT3	bedrock	37.4435	118.4909	1496
05BT4	bedrock high[a]	37.4236	118.4262	1365
05BT6	bedrock	37.4236	118.4262	1365
05BT8	bedrock	37.4233	118.4264	1369
05BT9	bedrock	37.4264	118.4253	1366
05BT15	bedrock	37.4142	118.4555	1387
05BT16	bedrock	37.4126	118.4696	1368
05BT17	bedrock	37.4130	118.4645	1376
05BT18	bedrock high[a]	37.4162	118.4566	1395
05BT19	bedrock	37.4162	118.4566	1394
05BT20	bedrock	37.4466	118.3998	1411

[a]bedrock high refers to a part of bedrock that is elevated above the surrounding surface.

Table 2: Results of stable Al analysis for all quartz samples and five duplicate analyses

Sample ID	**Standard addition Hannover** [a]				**Stand. addition GFZ (duplicate)** [b]	**Calibr. curve GFZ (duplicate)** [c]
	Number of additions considered	MSWD	Proba-bility	Al in sample solution (mg) [d]	Al in sample solution (mg) [d]	Al in sample solution (mg) [d]
05BT1	4	1.0	0.39	1.40 ± 0.11	1.325 ± 0.014	1.232 ± 0.030
05BT2	4	0.44	0.73	1.419 ± 0.094		
05BT3	5	0.35	0.85	1.78 ± 0.10		
05BT4	5	0.23	0.92	1.699 ± 0.074		
05BT6	5	0.35	0.84	1.253 ± 0.066		
05BT8	4	1.4	0.23	1.486 ± 0.091		
05BT9	4	0.39	0.76	1.293 ± 0.097	1.289 ± 0.012	1.196 ± 0.013
05BT15	4	0.076	0.97	1.219 ± 0.073		
05BT16	4	0.090	0.97	1.389 ± 0.092	1.338 ± 0.035	1.218 ± 0.024
05BT17	4	0.063	0.98	1.174 ± 0.072	1.172 ± 0.017	1.089 ± 0.013
05BT18	4	0.16	0.93	1.414 ± 0.065		
05BT19	4	0.27	0.85	1.291 ± 0.066	1.372 ± 0.012	1.2174 ± 0.0086
05BT20	3	0.88	0.42	1.954 ± 0.094		

[a.] Analysed by standard addition using the 167 nm wavelength.
[b.] Analysed by standard addition using the 396 nm wavelength.
[c.] Analysed by applying an ordinary calibration curve using the 396 nm wavelength.
[d.] For samples analysed in Hannover, the error (2σ) includes the error of the ICP-OES analysis and an estimated error of 1% for each added standard to account for the uncertainty caused by weighing and evaporation. Note that errors on the duplicate analyses (2σ) only include the analytical error.

Table 3: Measured concentrations of cosmogenic ^{21}Ne, ^{10}Be, and ^{26}Al in quartz from the Bishop Tuff, California

Sample ID	**^{21}Ne** (10^6 at/g)	**^{10}Be** (10^6 at/g)	**^{10}Be** (10^6 at/g)	**^{26}Al** (10^6 at/g)
	–	$t_{½}$ 1.51 Ma	$t_{½}$ 1.39 Ma	$t_{½}$ 0.72 Ma
05BT1	21.4 ± 1.1	5.02 ± 0.39 x	4.63 ± 0.36 x	32.0 ± 4.4
05BT2	23.1 ± 1.2	4.56 ± 0.36 x	4.20 ± 0.33 x	30.0 ± 4.0
05BT3	22.7 ± 1.1	4.71 ± 0.37 x	4.34 ± 0.34 x	32.5 ± 4.2
05BT4	18.2 ± 1.1	3.98 ± 0.57 y	3.67 ± 0.53 y	27.4 ± 3.4
05BT6	19.3 ± 1.2	4.40 ± 0.34 x	4.05 ± 0.32 x	26.4 ± 3.4
05BT8	17.34 ± 0.79 *	4.03 ± 0.46 y	3.71 ± 0.42 y	27.6 ± 3.9
05BT9	22.9 ± 1.3	4.66 ± 0.51 y	4.29 ± 0.47 y	27.9 ± 3.7
05BT15	16.99 ± 0.93	3.40 ± 0.41 y	3.13 ± 0.37 y	22.6 ± 3.0
05BT16	12.28 ± 0.84	2.68 ± 0.23 x	2.46 ± 0.21 x	16.6 ± 2.3
05BT17	11.05 ± 0.49 *	2.75 ± 0.25 x	2.53 ± 0.23 x	15.1 ± 2.0
05BT18	17.52 ± 0.95	3.78 ± 0.30 x	3.48 ± 0.28 x	25.2 ± 3.2
05BT19	18.0 ± 1.2	4.12 ± 0.32 x	3.79 ± 0.30 x	26.7 ± 3.4
05BT20	21.7 ± 1.4	4.57 ± 0.36 x	4.21 ± 0.33 x	29.5 ± 3.7

All errors are 2σ.
* Weighted mean of duplicate or triplicate analysis.
^{X} ^{9}Be concentration of carrier solution is 1052 ppm.
^{Y} ^{9}Be concentration of carrier solution is 405.4 ppm.

Table 4: Conservative maximum ranges for the mass removal rate, the factor f (cf. equations 1 and 3), and the $^{10}Be/^{21}Ne$ and $^{26}Al/^{21}Ne$ production ratios (for two ^{10}Be half-lives of 1.51 and 1.39 Ma)

Sample ID	Mass removal ratea	f 10/21	f 10/21	f 26/21	Production ratio P_{10}/P_{21} b	Production ratio P_{10}/P_{21} b	Production ratio P_{26}/P_{21} b
	g cm -2 Ma -1	t½ 1.51 Ma	t½ 1.39 Ma	t½ 0.72 Ma	t½ 1.51 Ma	t½ 1.39 Ma	t½ 0.72 Ma
05BT1	210-450	1.130-1.156	1.141-1.170	1.265-1.334	0.241-0.297	0.224-0.276	1.61-2.29
05BT2	170-400	1.135-1.161	1.146-1.175	1.278-1.347	0.204-0.251	0.189-0.234	1.42-2.01
05BT3	180-410	1.134-1.160	1.145-1.175	1.276-1.346	0.214-0.263	0.198-0.245	1.58-2.20
05BT4	240-490	1.127-1.153	1.138-1.166	1.257-1.326	0.208-0.291	0.193-0.271	1.62-2.26
05BT6	210-450	1.130-1.156	1.141-1.170	1.265-1.335	0.233-0.290	0.216-0.271	1.49-2.09
05BT8	270-530	1.124-1.149	1.134-1.162	1.248-1.316	0.229-0.300	0.213-0.279	1.69-2.41
05BT9	120-340	1.141-1.168	1.153-1.183	1.294-1.365	0.204-0.267	0.190-0.249	1.35-1.91
05BT15	290-550	1.122-1.147	1.132-1.160	1.243-1.310	0.195-0.260	0.181-0.242	1.42-1.99
05BT16	480-820	1.106-1.127	1.114-1.138	1.198-1.258	0.214-0.273	0.199-0.254	1.37-1.96
05BT17	560-930	1.101-1.121	1.108-1.131	1.184-1.240	0.246-0.307	0.228-0.285	1.39-1.94
05BT18	270-530	1.123-1.149	1.133-1.162	1.247-1.314	0.219-0.272	0.203-0.253	1.55-2.15
05BT19	260-510	1.125-1.150	1.135-1.163	1.251-1.319	0.231-0.291	0.215-0.271	1.60-2.25
05BT20	170-400	1.135-1.162	1.147-1.176	1.279-1.349	0.215-0.270	0.200-0.252	1.50-2.10

[a.] Calculated assuming a ^{21}Ne production rate of 19 at g^{-1} a^{-1} ±20%. For further explanation see section 4.3.
[b.] Ranges for the production ratio include the analytical uncertainties (2σ) of both nuclide concentrations.

Table 5: Production ratios and absolute production rates of ^{10}Be, ^{21}Ne and ^{26}Al (P_{10}, P_{21} and P_{26}; normalised to sea level and high latitude, in at g^{-1} a^{-1}) as derived from this study. Stated production rate uncertainties do not include that of the ^{10}Be production rate.

	^{10}Be half-life 1.51 Ma	^{10}Be half-life 1.39 Ma
Production ratios:		
P_{10}/P_{21}	0.249 ± 0.009	0.232 ± 0.009
P_{26}/P_{21}	1.80 ± 0.09	1.80 ± 0.09
P_{26}/P_{10}	7.23 ± 0.45	7.76 ± 0.49
Production rates according to Dunai (2000) scaling:		
P_{10}	5.01	4.61
P_{26}	20.10 ± 0.73	19.86 ± 0.77
P_{26}	36.2 ± 2.2	35.7 ± 2.3
Production rates according to Stone (2000) scaling:		
P_{10*}	5.07	4.66
P_{26}	20.35 ± 0.74	20.10 ± 0.78
P_{26}	36.6 ± 2.3	36.2 ± 2.3

* ^{10}Be production rates are based on Table 6 of Balco et al. (2008), where "reference production rates for spallation" are given for various scaling schemes. To obtain the total production rate, we have added a 2.1% contribution by negative muon interactions (Heisinger et al., 2002a) to those values.


a


b


c


d


e


f

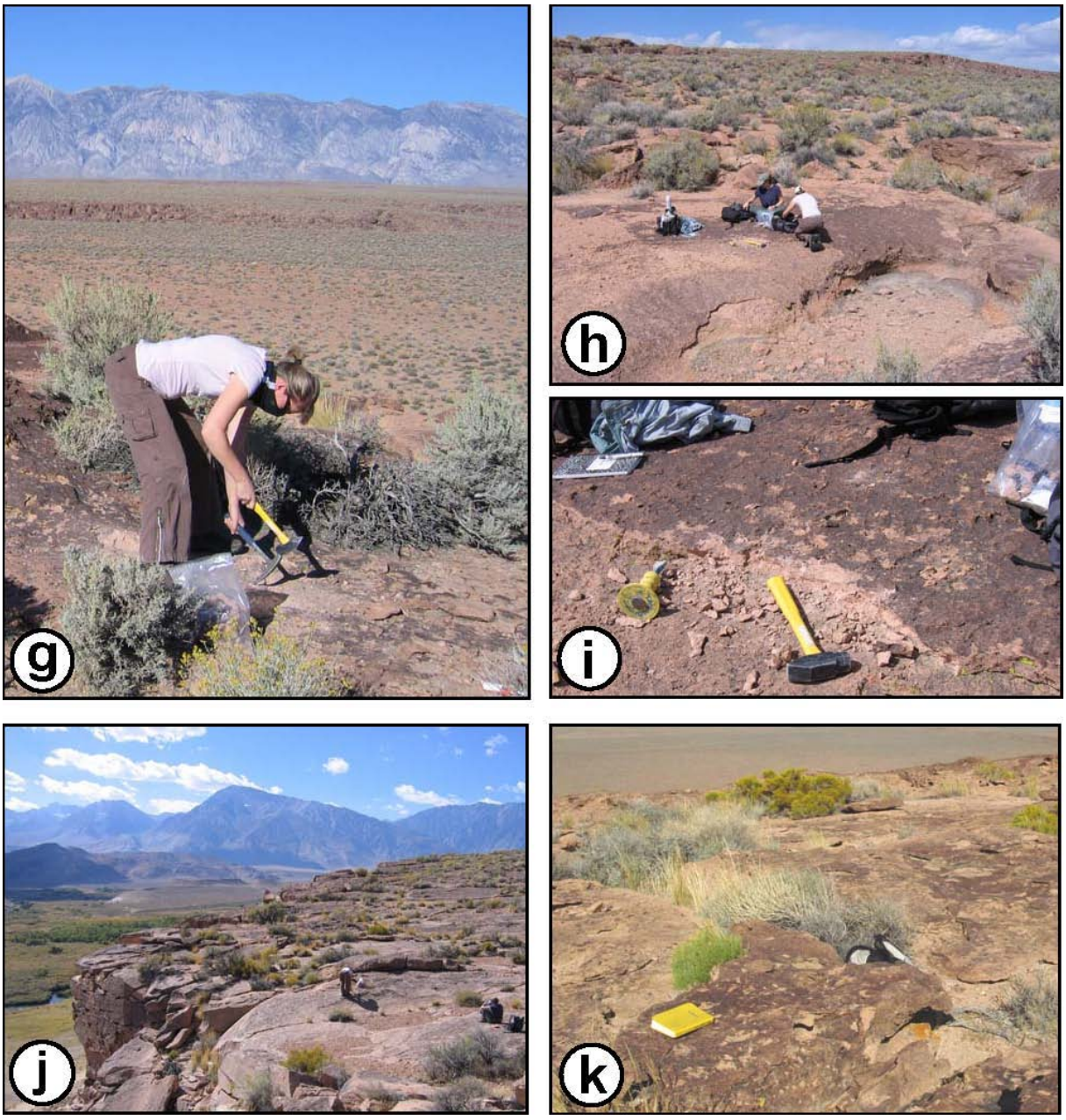

Figure S1: Field photographs of sample sites in the Volcanic Tableland of the Bishop Tuff, where ignimbrite samples were collected from bedrock outcrops. For geographic coordinates of the sample sites see Table 1; additional images are provided in Goethals et al. (2009). Samples 05BT1 (**a**,**b**), 05BT2 (**c**,**d**) and 05BT3 (**e**,**f**) were taken from flat bedrock surfaces with well developed dark desert varnish. Length of yellow chisel is 20 cm. **(g)** Bedrock surface from which MG collects sample 05BT8 is seen in the foreground. An ~10-m-high bedrock fault scarp is present in the centre of the image. The mountain range in the background belongs to the Sierra Nevada. View is toward the west. (**h**) This image provides an overview of the ephemeral channel where sample 05BT16 was taken. The dry pool in the foreground is situated ~0.6 m below the sampled bedrock surface. View is toward the northwest. (**i**) Sampled bedrock surface of 05BT16, which is coated with dark desert varnish. (**j**) Overview of another ephemeral channel, where MG takes sample 05BT17. Sample site is located just north of the steep cliff formed by the incision of Owens River, which is seen near the left edge of the image. The mountain range in the background belongs to the Sierra Nevada. View is toward the west. (**k**) Varnished bedrock surface from which sample 05BT20 was collected. Sample was taken just to the right of the yellow fieldbook, which is ~20 cm long. View is toward the northwest.